




Higgs pair production in the 2HDM: impact of loop corrections to the trilinear Higgs couplings and interference effects on experimental limits

S. Heinemeyer^{1,a}, M. Mühlleitner^{2,b}, K. Radchenko^{3,c} , G. Weiglein^{3,4,d}

¹ Instituto de Física Teórica (UAM/CSIC), Universidad Autónoma de Madrid, Cantoblanco, 28049 Madrid, Spain

² Institute for Theoretical Physics, Karlsruhe Institute of Technology, 76128 Karlsruhe, Germany

³ Deutsches Elektronen-Synchrotron DESY, Notkestr. 85, 22607 Hamburg, Germany

⁴ II. Institut für Theoretische Physik, Universität Hamburg, Luruper Chaussee 149, 22761 Hamburg, Germany

Received: 18 July 2024 / Accepted: 26 March 2025
© The Author(s) 2025

Abstract The results obtained at the LHC for constraining the trilinear Higgs self-coupling of the detected Higgs boson at about 125 GeV, λ_{hhh} , via the Higgs pair production process have significantly improved during the last years. We investigate the impact of potentially large higher-order corrections and interference effects on the comparison between the experimental results and the theoretical predictions for the pair production of the 125 GeV Higgs boson at the LHC. We use the theoretical framework of the Two Higgs Doublet Model (2HDM), containing besides the SM-like \mathcal{CP} -even Higgs boson h a second \mathcal{CP} -even Higgs boson H , which we assume to be heavier, $m_H > m_h$. We analyze in particular the invariant mass distribution of the two produced Higgs bosons and show that the loop corrections to the trilinear Higgs couplings λ_{hhh} and λ_{hhH} as well as interference contributions give rise to important effects both for the differential and the total cross section. We point out the implications for the experimental limits that can be obtained in the 2HDM for the case of the resonant production of the heavy Higgs boson H . We emphasize the importance of the inclusion of interference effects between resonant and non-resonant contributions in the experimental analysis for a reliable determination of exclusion bounds for a heavy resonance of an extended Higgs sector.

1 Introduction

After the discovery of a new scalar particle with a mass of about 125 GeV by ATLAS and CMS in 2012 [1–3], several of its properties have meanwhile been measured with a remarkable precision. From the results in particular for its couplings to the third generation fermions and to the massive gauge bosons it can be inferred that within the present experimental and theoretical uncertainties the predictions for the Higgs sector of the Standard Model (SM) are in good agreement with the experimental data [4,5]. The same is true, however, also for many scenarios of physics beyond the SM (BSM), which are motivated by the open questions and shortcomings of the SM.

While no conclusive sign of BSM physics has been discovered so far, extended scalar sectors, featuring parameter regions that are in agreement with all experimental and theoretical constraints, are particularly appealing in this context. Scalar particles play a fundamental role in the proposed answers to several open issues of the SM. In this regard, the determination of the shape of the Higgs potential is crucial for a better understanding of electroweak symmetry breaking [6,7] and of the thermal history of the universe. The current knowledge of the Higgs potential, which in the case of an extended Higgs sector is a complicated function of the components of all involved scalar fields, is limited to the distance in field space of the electroweak vacuum from the origin, given by the vacuum expectation value (vev), $v \approx 246$ GeV, and the curvature around it, given by the mass of the detected Higgs boson of about 125 GeV. The information gathered on the trilinear Higgs coupling (THC) is, however, insufficient

^a e-mail: Sven.Heinemeyer@cern.ch

^b e-mail: margarete.muehlleitner@kit.edu

^c e-mail: kateryna.radchenko@desy.de (corresponding author)

^d e-mail: georg.weiglein@desy.de

so far to determine whether a BSM Higgs sector is realized in nature.

Among the most prominent shortcomings of the SM is its inability to explain the observed baryon asymmetry of the universe (BAU) [8]. A dynamical explanation is given by electroweak baryogenesis (EWBG) [9–17], provided the three Sakharov conditions [18] are fulfilled. Among these is the departure from thermal equilibrium. A large barrier in the Higgs potential at the electroweak (EW) phase transition, which can arise from a sizable THC, enables a strong first order EW phase transition (SFOEWPT), and thus helps to facilitate baryogenesis [19–22]. Accordingly, the realization of an SFOEWPT is often correlated with a significant enhancement (of at least 20–30%) of the THC of the detected Higgs boson, λ_{hhh} , compared to the SM prediction [19, 23–25]. The contributions giving rise to an SFOEWPT and a shift in the prediction for λ_{hhh} can generically occur in models with extended Higgs sectors via the higher-order corrections involving additional heavy states [19, 26]. It has been demonstrated that in simple extensions such as the Two Higgs Doublet Model (2HDM) the loop corrections to λ_{hhh} can change the tree-level value by several 100% while being in agreement with all existing experimental and theoretical constraints [26, 27]. Therefore already the present experimental information on λ_{hhh} (see below) provides an important test of the allowed parameter space [27].

Defining by κ_λ the coupling modifier relative to the tree-level THC in the SM,

$$\kappa_\lambda \equiv \frac{\lambda_{hhh}}{\lambda_{\text{SM}}^{(0)}}, \quad (1)$$

with

$$\lambda_{\text{SM}}^{(0)} = \frac{m_h^2}{2v^2} \simeq 0.13, \quad (2)$$

the current experimental sensitivity to the 125 GeV Higgs self-interaction constrains the THC to be inside the range $-0.4 < \kappa_\lambda < 6.3$ at 95% C.L. (ATLAS [28]) and $-1.24 < \kappa_\lambda < 6.49$ at 95% C.L. (CMS [4]), using mainly the information from the search for the Higgs pair production process, where an SM-like top-Yukawa coupling is assumed. While the current sensitivity is still far from the SM (tree-level) value of $\kappa_\lambda = 1$, the existing limits already probe large deviations from this value that can occur in simple extensions of the SM Higgs sector such as the 2HDM [27].

The Large Hadron Collider in its High Luminosity phase (HL-LHC) will be able to significantly improve the sensitivity to possible BSM scenarios [29]. Current prospects for the sensitivity at the HL-LHC with 3 ab^{-1} integrated luminosity per detector are $-0.5 < \kappa_\lambda < 1.6$ at the 1σ level in the combination of the $b\bar{b}b\bar{b}$, $b\bar{b}\gamma\gamma$ and $b\bar{b}\tau^+\tau^-$ channels [30]. This on the one hand motivates precise theoretical predictions for the Higgs pair production process, which at the (HL-)LHC

is dominantly given by gluon fusion into Higgs pairs, taking into account the possibility of sizable BSM contributions to the occurring trilinear Higgs couplings. On the other hand it is important to ensure that the obtained experimental bounds on the gluon fusion Higgs pair production process can be confronted in a meaningful way with theoretical predictions in different scenarios of electroweak symmetry breaking, where a resonant contribution from the exchange of a heavy neutral Higgs boson might be possible in addition to the non-resonant contributions that are always present. The latter contain in particular a contribution involving the Higgs boson at 125 GeV and a top-loop induced contribution where no Higgs boson enters at leading order.

In this paper we adopt the well motivated 2HDM as theoretical framework, but we stress that our qualitative results are applicable to a wide class of extended Higgs sectors. We will investigate in particular the effects of two contributions entering the process of gluon fusion into Higgs pairs, $gg \rightarrow hh$, which provides direct access to λ_{hhh} at the LHC. We will study the impact of the inclusion of a possible resonant heavy Higgs contribution with subsequent decay into a pair of the Higgs boson at 125 GeV, involving the trilinear Higgs coupling λ_{hhH} at lowest order. Furthermore, we will investigate the effect of potentially large higher-order corrections to λ_{hhh} and λ_{hhH} on the Higgs pair production process. We will demonstrate that the combination of the two effects has important implications on the experimental limits that can be extracted from the Higgs pair production process.

Our paper is organized as follows. In Sect. 2 we describe the 2HDM in more detail and summarize the predictions for the trilinear Higgs couplings at tree level (Sect. 2.2) and at one-loop order (Sect. 2.3). We briefly review 2HDM Higgs pair production at the LHC in Sect. 3.1. We present our results for the differential cross section w.r.t. the invariant mass in Sect. 3.2. The confrontation of the Higgs pair production process with experimental limits is discussed in Sect. 4, focusing on the case of non-resonant production in Sect. 4.1 and on the case of resonant production in Sect. 4.2. Our conclusions are given in Sect. 5.

2 Trilinear Higgs couplings in the 2HDM

2.1 Model details

One of the simplest scalar extensions of the SM is the addition of one complex doublet under the SU(2) symmetry, resulting in the 2HDM. For simplicity, we assume a \mathcal{CP} -conserving 2HDM [31–34]. The tree-level scalar potential with a \mathbb{Z}_2 symmetry, under which the two complex Higgs doublet fields transform as $\Phi_1 \rightarrow \Phi_1$ and $\Phi_2 \rightarrow -\Phi_2$, is given by

$$V = m_{11}^2(\Phi_1^\dagger \Phi_1) + m_{22}^2(\Phi_2^\dagger \Phi_2) - m_{12}^2(\Phi_1^\dagger \Phi_2 + \Phi_2^\dagger \Phi_1)$$

$$\begin{aligned}
& + \frac{\lambda_1}{2} (\Phi_1^\dagger \Phi_1)^2 + \frac{\lambda_2}{2} (\Phi_2^\dagger \Phi_2)^2 \\
& + \lambda_3 (\Phi_1^\dagger \Phi_1) (\Phi_2^\dagger \Phi_2) + \lambda_4 (\Phi_1^\dagger \Phi_2) (\Phi_2^\dagger \Phi_1) \\
& + \frac{\lambda_5}{2} [(\Phi_1^\dagger \Phi_2)^2 + (\Phi_2^\dagger \Phi_1)^2],
\end{aligned} \quad (3)$$

with all coupling and mass parameters being real. The \mathbb{Z}_2 symmetry is softly broken by the parameter m_{12}^2 . The fields Φ_1 and Φ_2 can be conveniently parametrized as

$$\begin{aligned}
\Phi_1 &= \begin{pmatrix} \phi_1^+ \\ \frac{1}{\sqrt{2}}(v_1 + \rho_1 + i\eta_1) \end{pmatrix}, \\
\Phi_2 &= \begin{pmatrix} \phi_2^+ \\ \frac{1}{\sqrt{2}}(v_2 + \rho_2 + i\eta_2) \end{pmatrix},
\end{aligned} \quad (4)$$

in terms of their respective vacuum expectation values, v_1 and v_2 (with $\sqrt{v_1^2 + v_2^2} \equiv v$), and the interaction fields $\phi_{1,2}^\pm$, $\rho_{1,2}$ and $\eta_{1,2}$ that mix to give rise to five physical scalar fields and three (would-be) Goldstone bosons. The physical fields comprise two \mathcal{CP} -even fields, h and H , where by convention $m_h < m_H$, and we identify h with the scalar boson observed at the LHC at about 125 GeV, one \mathcal{CP} -odd field, A , and one charged Higgs pair, H^\pm . The mixing matrices diagonalizing the \mathcal{CP} -even and \mathcal{CP} -odd/charged Higgs mass matrices can be expressed in terms of the mixing angles α and β , respectively, with $t_\beta \equiv v_2/v_1$ ¹. The “alignment limit” [35] corresponds to $c_{\beta-\alpha} \rightarrow 0$, where the light Higgs boson h has couplings to fermions and gauge bosons at lowest order that exactly correspond to the ones in the SM.

The occurrence of tree-level flavor-changing neutral currents (FCNC) is avoided by extending the \mathbb{Z}_2 symmetry to the Yukawa sector. This results in four variants of the 2HDM, depending on the \mathbb{Z}_2 parities of the fermion types. In this article we focus on the Yukawa type I, where all fermions couple to Φ_2 . The couplings of the Higgs bosons to SM particles are determined by the mixing in the scalar sector. The couplings of the neutral \mathcal{CP} -even Higgs bosons to fermions are given by

$$\mathcal{L} = - \sum_{f=u,d,l} \frac{m_f}{v} \left[\xi_h^f \bar{f} f h + \xi_H^f \bar{f} f H \right], \quad (5)$$

where m_f are the fermion masses, and $\xi_{h,H}^f$ are the fermionic Yukawa coupling modifiers, which express the couplings relative to the ones of the SM Higgs. They are equal for all three generations of up-type quarks (u), down-type quarks (d) and leptons (l). In the type I 2HDM the coupling modifiers are equal for all fermions and given by ($f = t, b, \tau$),

$$\xi_h^f = s_{\beta-\alpha} + c_{\beta-\alpha} \cot \beta, \quad \xi_H^f = c_{\beta-\alpha} - s_{\beta-\alpha} \cot \beta. \quad (6)$$

¹ We use the short-hand notation $s_x \equiv \sin x$, $c_x \equiv \cos x$, $t_\beta \equiv \tan \beta$.

The Yukawa hierarchy implies that the Higgs boson couples predominantly to the top quark (t) and to a lesser extent to the bottom quark (b).

We work in the physical basis of the 2HDM, where the Higgs potential parameters are expressed in terms of a set of parameters given mostly by physical quantities as

$$c_{\beta-\alpha}, t_\beta, v, m_h, m_H, m_A, m_{H^\pm}, m_{12}^2. \quad (7)$$

Here, m_h, m_H, m_A, m_{H^\pm} are the masses of the physical scalars.

2.2 Tree-level trilinear Higgs couplings in the 2HDM

The generic tree-level THCs $\lambda_{h h_i h_j}^{(0)}$ involving at least one Higgs boson h with $m_h \sim 125$ GeV are defined such that the Feynman rules are given by

$$\begin{array}{c}
h_i \\
\diagup \quad \diagdown \\
h \text{ --- } \quad \quad \quad \\
\diagdown \quad \diagup \\
h_j
\end{array} = -i v n! \lambda_{h h_i h_j}^{(0)}, \quad (8)$$

where n is the number of identical particles in the vertex. For our analysis in the following the two couplings λ_{hhh} and λ_{hhH} are relevant. With the convention given in Eq. (8) the self-coupling $\lambda_{hhh}^{(0)}$ has the same normalization at tree-level as in the SM, where the Feynman rule is given by $-6i v \lambda_{\text{SM}}^{(0)}$. The 2HDM tree-level THCs $\lambda_{hhh}^{(0)}$ and $\lambda_{hhH}^{(0)}$ can be cast into the forms

$$\begin{aligned}
\lambda_{hhh}^{(0)} &= -\frac{1}{2} \left\{ \lambda_1 c_\beta s_\alpha^3 - \lambda_2 c_\alpha^3 s_\beta + (\lambda_3 + \lambda_4 + \lambda_5) \right. \\
&\quad \times \left. \left(c_\alpha^2 c_\beta s_\alpha - c_\alpha s_\alpha^2 s_\beta \right) \right\} \\
&= \frac{1}{2v^2} \left\{ m_h^2 s_{\beta-\alpha}^3 + \left(3m_h^2 - 2\bar{m}^2 \right) c_{\beta-\alpha}^2 s_{\beta-\alpha} \right. \\
&\quad \left. + 2 \cot 2\beta \left(m_h^2 - \bar{m}^2 \right) c_{\beta-\alpha}^3 \right\}, \\
\lambda_{hhH}^{(0)} &= \frac{1}{2} \left\{ 3\lambda_1 c_\alpha c_\beta s_\alpha^2 + 3\lambda_2 c_\alpha^2 s_\alpha s_\beta \right. \\
&\quad \left. + (\lambda_3 + \lambda_4 + \lambda_5) \left(c_\alpha^3 c_\beta - 2c_\alpha^2 s_\alpha s_\beta \right. \right. \\
&\quad \left. \left. - 2c_\alpha c_\beta s_\alpha^2 + s_\alpha^3 s_\beta \right) \right\} \\
&= -\frac{c_{\beta-\alpha}}{2v^2} \left\{ \left(2m_h^2 + m_H^2 - 4\bar{m}^2 \right) s_{\beta-\alpha}^2 \right. \\
&\quad \left. + 2 \cot 2\beta \left(2m_h^2 + m_H^2 - 3\bar{m}^2 \right) s_{\beta-\alpha} c_{\beta-\alpha} \right\}
\end{aligned} \quad (9)$$

$$-\left(2m_h^2 + m_H^2 - 2\bar{m}^2\right)c_{\beta-\alpha}^2\}, \quad (10)$$

where \bar{m}^2 is defined as

$$\bar{m}^2 = \frac{m_{12}^2}{s_\beta c_\beta}. \quad (11)$$

From the latter expressions one can easily read off the THCs in the alignment limit where $c_{\beta-\alpha} = 0$, namely $\lambda_{hhh}^{(0)} = \lambda_{\text{SM}}^{(0)}$ and $\lambda_{hhH}^{(0)} = 0$. Away from the alignment limit the predictions for these couplings in the 2HDM, even at tree level, can be significantly modified, see e.g. Refs. [36–38] for studies in all four Yukawa types.

2.3 Loop-corrected trilinear Higgs couplings

In the 2HDM, it has been shown that the loop contributions to the THCs involving the heavy BSM Higgs bosons can give rise to corrections of the order of 100% and larger [26,39] w.r.t. their tree-level values. More recently, also two-loop corrections have been computed [40] enhancing in some parts of the parameter space the value of κ_λ to the sensitivity of current and future runs of the LHC [27]. The occurrence of large loop corrections should, however, not be regarded as a sign of the breakdown of perturbation theory, as large corrections at one-loop order are present mainly due to new contributions involving couplings of the Higgs boson h to heavier BSM Higgs bosons that do not appear at tree level [26], while the size of the two-loop corrections relative to the one-loop result follows the expected perturbative behavior [27,40,41]. In view of these findings the impact of these large higher-order corrections on the Higgs pair production process should be studied.

For the computation of the one-loop corrections to the THCs contributing to our numerical analysis we use the public code BSMPT [42,43], where the trilinear Higgs couplings are extracted from the one-loop corrected effective potential (evaluated here at zero temperature),

$$V_{\text{eff}} = V_{\text{tree}} + V_{\text{CW}} + V_{\text{CT}}. \quad (12)$$

In this equation, V_{tree} is the tree-level potential of the 2HDM given in Eq. (3), V_{CW} is the one-loop Coleman–Weinberg potential [44,45] at zero temperature, and V_{CT} is the counterterm potential. The counterterm potential is chosen such that the masses and mixing angles are kept at their tree-level values, which therefore allows us to conveniently use them as inputs in our scans. In this set-up, the “effective loop-corrected trilinear Higgs couplings” can be computed as the third derivatives of the effective potential with respect to the Higgs fields, evaluated at the minimum,

$$\lambda_{hhh}^{(1)} = \frac{1}{3!v} \frac{\partial^3 V_{\text{eff}}}{\partial h^3} \Big|_{h,H=0}, \quad \lambda_{hhH}^{(1)} = \frac{1}{2!v} \frac{\partial^3 V_{\text{eff}}}{\partial h^2 \partial H} \Big|_{h,H=0}. \quad (13)$$

Alternatively, one could use a fully diagrammatic approach by calculating the one-loop corrections with the public tool anyH3 [46], where the extension of the provided results for $\lambda_{hhh}^{(1)}$ to $\lambda_{hhH}^{(1)}$ and further trilinear Higgs couplings is currently under development.

3 Higgs pair production in the 2HDM

3.1 Theoretical introduction

The trilinear Higgs boson self-coupling is directly accessible in Higgs pair production. At the LHC, the dominant process is gluon fusion into Higgs pairs, which at leading order is mediated by heavy quark loops, see Fig. 1. The bottom quark contribution in the SM only plays a subleading role, whereas in the 2HDM it can be enhanced by large values of t_β , depending on the Yukawa type. The THCs enter through the s -channel diagrams, as shown in the first two diagrams of Fig. 1. In the SM, the triangle and box diagrams interfere destructively leading to a relatively small cross section of $\sigma_{\text{SM}} = 31.05^{+6\%}_{-23\%}$ fb at 13 TeV center-of-mass energy [47,48].² The LO QCD value at 13 TeV, which is the energy we use for all the plots shown in the paper, is $\sigma_{\text{SM}} = 16.6$ fb, and the NLO QCD value in the Born improved heavy-top limit is 32.7 fb.

In the 2HDM, there are two potential sources of changes w.r.t. the SM. Firstly, the couplings in the SM-like diagrams can differ from the SM values. Whereas the top-Yukawa coupling is restricted by the current constraints to about $\pm 10\%$ the SM value, much larger deviations in the trilinear Higgs self-coupling λ_{hhh} are possible in accordance with all relevant constraints [27,37]. Changes in λ_{hhh} can modify the interference of the SM-like triangle and box diagrams. Secondly, there is an additional s -channel contribution from the heavy Higgs boson, involving the trilinear coupling λ_{hhH} and the top Yukawa coupling of the H . In case the mass m_H exceeds twice the mass of the lighter Higgs boson,

² This is the value obtained at NNLO_FTapprox for $m_h = 125$ GeV with the renormalization and factorization scale chosen to be half the invariant Higgs pair mass for a c.m. energy of $\sqrt{s} = 13$ TeV [47]. At NNLO_FTapprox, the cross section is computed at next-to-next-to-leading order (NNLO) QCD in the heavy-top limit [49–51] with full leading order (LO) and next-to-leading order (NLO) mass effects [48, 52–55] and full mass dependence in the one-loop double real corrections at NNLO QCD. The uncertainty combines the uncertainty from the renormalization and factorization scale variations with the uncertainty due to the choice of the renormalization scheme and scale of the mass of the top quark [48].

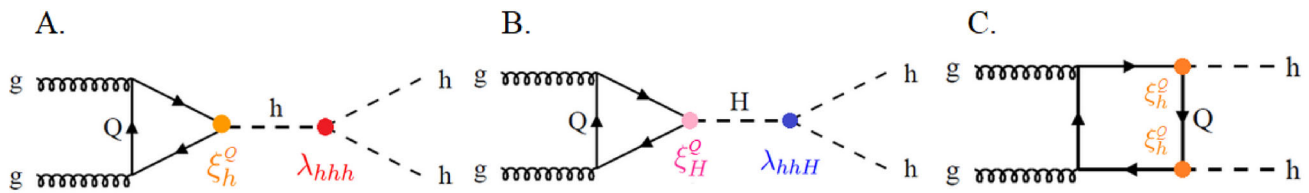


Fig. 1 Generic diagrams contributing to the pair production of the Higgs boson h at about 125 GeV in gluon fusion within the 2HDM, mediated by heavy quark loops, $Q = t, b$. The red and blue dots denote the triple Higgs couplings λ_{hhh} and λ_{hhH} , respectively, evaluated at leading or next-to-leading order; the orange (pink) dot denotes the h

(H) Yukawa coupling parametrized by the coupling modifier ξ_h^Q (ξ_H^Q). The diagrams labelled as A and C are the continuum diagrams, which appear in analogous form in the SM. The diagram labelled B is the resonant diagram, involving the s -channel heavy H exchange

$m_H > 2m_h \sim 250$ GeV, this contribution can lead to resonant hh production, in which case the corresponding diagram is referred to as “resonant diagram”. Thereby, the cross section can be significantly enhanced. On the other hand, depending on the involved couplings and masses, there can also be destructive interferences between the triangle diagrams of the h and H exchange and the box diagram. Accordingly, the loop contributions to the trilinear Higgs couplings are expected to have an important impact both on the prediction for the inclusive cross section and also for the shape of the invariant mass distributions, as will be discussed in the next section.

In this work, we include for the first time in the 2HDM³ the one-loop corrections to the triple Higgs couplings in the computation of Higgs pair production and analyze their effects. It should be noted that in the effective trilinear coupling approach, as defined above, the couplings are evaluated in the approximation of vanishing external momenta. Taking into account the appropriate momentum dependence for the Higgs pair production process would be expected to modify the predictions for the total di-Higgs production cross section only at the percent level in the 2HDM type I [46]. Furthermore, the loop-corrected effective trilinear couplings constitute the leading contributions to the full EW corrections for scenarios in which the loop corrections to λ_{hhh} and/or λ_{hhH} are very large. In this case, contributions beyond the trilinear Higgs self-couplings, e.g. including additional powers of the top Yukawa couplings, can be shown to be sub-dominant [27]. Therefore, for the case of sizable loop corrections to the THCs our results should provide a good approximation to the full electroweak loop corrections to the inclusive process at this order.

In regions where these corrections are relatively small, which for the non-resonant case implies that the predicted cross sections are significantly below the current experimental sensitivity, this approach becomes less accurate and

a complete next-to-leading-order (NLO) electroweak (EW) calculation of the cross section would be required, which is beyond the scope of this work.⁴ The aim of our work, on the other hand, is an analysis of possible implications of large loop contributions and interference effects, in particular regarding the interpretation of the experimental results. For this purpose the approximate approach pursued here should be sufficiently accurate.

For the numerical evaluation, we use the code HPAIR [37, 62–64], adapted to the 2HDM. This code was originally designed to compute within the SM and its Minimal Supersymmetric Extension (MSSM) the cross sections for the production of two neutral Higgs bosons through gluon fusion at the LHC. The calculations are carried out at leading order (LO) with the full top-quark mass dependence and include NLO QCD corrections, assuming the limit of an infinite top-quark mass and neglecting bottom loop contributions.⁵ However, in the 2HDM the latter assumption can become less accurate at large values of t_β due to the increased importance of the bottom quark loop contribution, depending on the Yukawa type. In the Yukawa type I, which is used throughout our analysis, no enhancement of the bottom Yukawa coupling occurs. Furthermore, for this analysis, we have modified HPAIR to include the one-loop corrections to the THCs as described in Sect. 2.3. The PDF set used in the numerical evaluation at LO (NLO) QCD is CT14lo (CT14nlo) [66].

3.2 Impact of loop corrections to the trilinear Higgs couplings on invariant mass distributions

In this section, we explore the behavior of the invariant mass distribution of the di-Higgs final state when incorporating loop corrections to the THCs involved in Higgs pair production. In Fig. 2 we present various m_{hh} distributions for a

³ For investigations of the effect in the SM, see Ref. [56], and in the next-to-minimal supersymmetric extension of the SM (NMSSM), see Refs. [57, 58].

⁴ For results on the NLO EW corrections to SM Higgs pair production, see Refs. [56, 59–61].

⁵ Recently, the full top-quark mass dependence at NLO QCD has been provided for the production of an hH pair as well as for a CP -odd Higgs pair in the 2HDM [65].

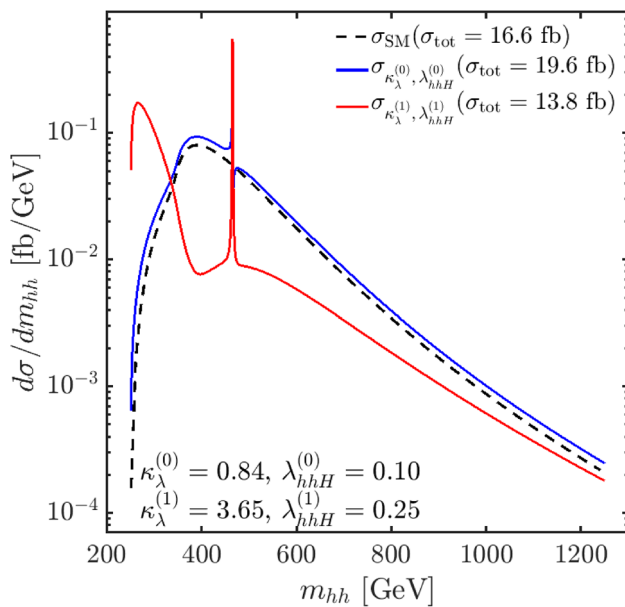


Fig. 2 Invariant mass distribution for the benchmark point in the 2HDM type I defined in Eq. (14). The SM prediction (dashed black line) is shown together with the 2HDM results with (solid blue line) and without (solid red line) loop corrections to the THC's, see text

sample benchmark point in the 2HDM of type I. It is defined by the input parameters

$$\begin{aligned} t_\beta &= 10, \quad c_{\beta-\alpha} = 0.13 \quad (s_{\beta-\alpha} > 0) \\ m_H &= 465 \text{ GeV}, \quad m_A = m_{H^\pm} = 660 \text{ GeV} \quad \text{and} \\ m_{12}^2 &= m_H^2 c_\alpha^2 / t_\beta. \end{aligned} \quad (14)$$

For this point we find

$$\begin{aligned} \kappa_\lambda^{(0)} &\equiv \frac{\lambda_{hhh}^{(0)}}{\lambda_{\text{SM}}^{(0)}} = 0.84, \quad \kappa_\lambda^{(1)} \equiv \frac{\lambda_{hhh}^{(1)}}{\lambda_{\text{SM}}^{(0)}} = 3.65, \\ \lambda_{hhH}^{(0)} &= 0.10 \quad \text{and} \quad \lambda_{hhH}^{(1)} = 0.25, \end{aligned} \quad (15)$$

and the rest of the trilinear couplings at tree level are:

$$\begin{aligned} \lambda_{hHH}^{(0)} &= -2.31, \quad \lambda_{HHH}^{(0)} = 0.07, \\ \lambda_{hAA/hH^\pm H^\pm}^{(0)} &= -5.83 \quad \text{and} \quad \lambda_{HAA/HH^\pm H^\pm}^{(0)} = 0.54. \end{aligned} \quad (16)$$

The THC of the SM-like Higgs boson is hence very SM-like at tree level, but substantially increased by one-loop corrections. The THC between the heavy Higgs boson and the two light Higgs bosons is increased by 150% by the one-loop corrections.

Concerning the invariant mass distributions shown in our analysis, it is important to note that they are calculated at leading order. It would be possible to compute the invariant mass spectrum with HPAIR at NLO QCD in the Born improved heavy-top limit. However, it has been shown that mass effects may significantly distort the NLO distributions

[48, 52–55]. While, for the 2HDM, the full mass effects at NLO QCD have been considered in Ref. [65], there exists no public code that allows us to obtain results for our benchmark scenarios, in particular including resonances. In Ref. [67] a parametrisation has been given for the total cross section and the m_{hh} distribution in the framework of a non-linear effective field theory as a function of the anomalous Higgs couplings that includes NLO corrections. While this framework considers deviations from the SM Higgs sector, it however does not include the possibility of additional Higgs bosons. Consequently, one has the choice between a LO distribution ignoring NLO effects and an approximate NLO distribution ignoring finite top-mass effects at NLO, where we chose to adopt the LO case. While this approach obviously cannot capture the full NLO mass effects, it does provide information regarding the possible impact of a BSM Higgs boson resonance and of NLO electroweak corrections to THC's on the m_{hh} distribution, which is the main goal of our analysis. The inclusive cross section, on the other hand, is rather well approximated at NLO QCD by applying a K -factor, obtained from the ratio of the NLO to the LO cross section, of $K(\text{NLO}) \approx 2$ [68].

The blue curve in Fig. 2 is the invariant mass distribution for the specified benchmark point with both THC's taken at tree-level, whereas the red line displays the result for the distribution for the case where both THC's are incorporated at the one-loop level. The dashed black line indicates the SM prediction. Starting our discussion with the tree-level distribution (blue line), several features can be noticed. The small values of the differential cross section just above the threshold are a consequence of a cancellation of the form factors involved in the continuum diagrams (diagrams A and C in Fig. 1). The invariant mass distribution reaches a maximum at $m_{hh} \approx 400$ GeV, which is related to the di-top on-shell production and is also present in the distribution of single Higgs production (see e.g. Ref. [69]). A further striking feature is the resonance located at $m_{hh} \approx m_H$ showing a peak-dip structure. Apart from the resonant contribution, the shape of the tree-level distribution resembles the SM prediction (dashed black line), taking into account the relatively small value of $\lambda_{hhh}^{(0)}$.

Turning to the red line, incorporating one-loop corrections to both THC's, one can observe that the shape of the distribution changes drastically. In particular the cancellation close to the kinematical threshold in the leading order distribution is lifted.⁶ This cancellation now happens at values of $m_{hh} \approx 400$ GeV and leads to a large reduction of the differential cross section in the region where at leading order a maximum occurred. Furthermore, close to the kinematical threshold the distribution is largely enhanced,

⁶ This effect has already been observed in the context of the SM in Ref. [56].

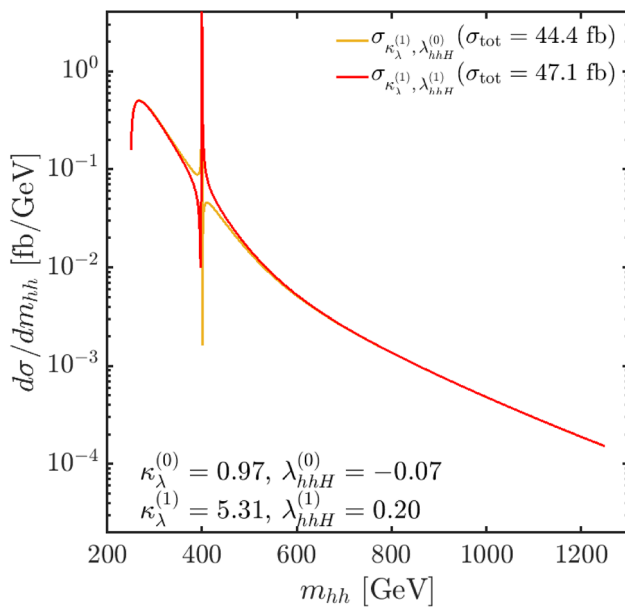


Fig. 3 Impact of the loop corrections to λ_{hhH} on the resonance shape for the benchmark point defined in Eq. (17). The red (orange) line shows the result with (without) loop corrections to λ_{hhH}

leading to the appearance of a structure resembling a peak at $m_{hh} \approx 250$ GeV. We also investigated the impact of the one-loop corrections to the two THCs individually (not shown in the plot) and found that in this scenario the corrections to λ_{hhH} play a minor role, while the biggest changes are caused by the large one-loop corrections to κ_λ .

Also shown in the figure are the total cross section values⁷. Here it is interesting to note that the decrease in the tree level value of κ_λ of about 15% w.r.t. the SM⁸ leads to an increase of roughly 20% of the tree level cross section, whereas the inclusion of the one-loop corrections to the THCs results in a reduction of the 2HDM cross section by about 30%, i.e. 20% smaller than the SM result.

In Fig. 3 we present an example where the loop corrections to λ_{hhH} play a crucial role. The input parameters are

$$\begin{aligned} t_\beta &= 15, \quad c_{\beta-\alpha} = 0.12 \quad (s_{\beta-\alpha} > 0), \\ m_H &= 400 \text{ GeV}, \quad m_A = m_{H^\pm} = 660 \text{ GeV} \quad \text{and} \\ m_{12}^2 &= m_H^2 s_\beta c_\beta. \end{aligned} \quad (17)$$

For these parameters we find

$$\begin{aligned} \kappa_\lambda^{(0)} &= 0.97, \quad \kappa_\lambda^{(1)} = 5.31, \quad \lambda_{hhH}^{(0)} = -0.07 \quad \text{and} \\ \lambda_{hhH}^{(1)} &= 0.20, \end{aligned} \quad (18)$$

⁷ The total cross section values are given at LO QCD in accordance with the distributions given at LO. As stated above, including the NLO QCD corrections obtained with HPAIR the cross section values would increase by about a factor of 2 [68].

⁸ Here we use the LO SM total cross section, σ_{SM} , as given in Sect. 3.1 for comparison.

and

$$\begin{aligned} \lambda_{hHH}^{(0)} &= -2.27, \quad \lambda_{HHH}^{(0)} = 0.12, \\ \lambda_{hAA/hH^\pm H^\mp}^{(0)} &= -6.77 \quad \text{and} \quad \lambda_{HAA/HH^\pm H^\mp}^{(0)} = 0.67. \end{aligned} \quad (19)$$

The result including NLO corrections only to κ_λ is shown as orange solid line, and corresponds to a total LO QCD cross section of 44.4 fb. The m_{hh} distribution shows a pronounced peak–dip structure at $m_{hh} \sim m_H$. The result including the one-loop corrections to both THCs is shown as solid red line. The incorporation of the higher-order corrections results in a larger $\lambda_{hhH}^{(1)}$ value with opposite sign compared to the tree-level value. Its inclusion gives rise to a dip–peak structure, i.e. the opposite behavior compared to the tree-level case. This effect is caused by a change in the overall sign of the couplings involved in the resonant diagram, $\lambda_{hhH} \times \xi_H^t$, as discussed in Ref. [68]. In the present example we demonstrate that such a change can arise solely from one-loop corrections to λ_{hhH} , i.e. the incorporation of electroweak loop corrections is crucial in this case for a reliable prediction of the experimental signature (experimental effects like smearing due to a limited detector resolution will be discussed in the next section). This effect is clearly visible even in the case of large one-loop corrections to κ_λ , as it is the case in this example. Our discussion highlights the relevance of higher-order corrections also in the THCs involving BSM Higgs bosons, as they can have a drastic effect on the invariant mass distributions.

4 Confrontation with experimental limits

In view of the significant improvements in the experimental sensitivity to the di-Higgs production cross section that have occurred recently and are expected to be achieved in the future it is crucial that the experimental limits (and of course eventually also the experimental measurements) are presented in such a way that they can be confronted with theoretical predictions in different scenarios of electroweak symmetry breaking in a well-defined way. Up to now the experimental limits presented by ATLAS and CMS are given either for non-resonant production, taking into account only SM-like contributions, or for purely resonant production, where SM-like non-resonant contributions are omitted. We discuss both types of limits in the following.

4.1 Non-resonant production

We start our discussion with the analysis of the non-resonant limits. In this case the experimental limits are obtained under the assumption that there is no contribution from an s -channel exchange of an additional Higgs boson, i.e. only the contributions of diagrams A and C in Fig. 1 are taken into account.

The most recent results from ATLAS [28] and CMS [4] report a limit on the cross section of $gg \rightarrow hh$, which depends on the value of κ_λ , and a bound on κ_λ is extracted. This is done by comparing the experimental limit with the SM prediction for a varied κ_λ . We show in Fig. 4 an example of the application of these limits for one particular benchmark scenario in the 2HDM, where we vary $c_{\beta-\alpha}$. The chosen input parameters are

$$t_\beta = 10, \quad c_{\beta-\alpha} \in \{0 \dots 0.16\} \quad (s_{\beta-\alpha} > 0), \quad (20)$$

$$m_H = m_A = m_{H^\pm} = 1000 \text{ GeV}, \quad m_{12}^2 = m_H^2 c_\alpha^2 / t_\beta.$$

The large m_H value ensures that the resonant contribution from the s -channel H exchange is negligible (we do not discuss effects of varying λ_{hhH} in this context). The variation of $c_{\beta-\alpha}$ results in a variation of κ_λ as indicated in the left plot of Fig. 4. The blue dashed line shows the prediction for κ_λ at lowest order, while the blue solid line shows the one-loop prediction for κ_λ . The gray line indicates the value of $\kappa_\lambda = 1$, which corresponds to a coupling value of $\lambda_{hhh} = \lambda_{\text{SM}}^{(0)}$. The parameter spaces that are excluded by theoretical constraints are indicated by the yellow (vacuum stability), dark green (perturbative unitarity at LO) and light green (perturbative unitarity at NLO) shaded areas. For the application of these limits we used the public package `2hdmTools` [70]. The constraints from vacuum stability exclude the displayed yellow region with negative values of $c_{\beta-\alpha}$. For the largest positive values of $c_{\beta-\alpha}$ the tightest bound arises from perturbative unitarity (for the constraints at LO and NLO we require that the eigenvalues of the $2 \rightarrow 2$ scattering matrix satisfy $|a_0| < 1$, where a_0 denotes the s -wave amplitude of the scattering process). Demanding that the measured properties of the Higgs boson at 125 GeV should be satisfied poses a bound that is weaker than the one from NLO perturbative unitarity and therefore this bound is not explicitly shown in the plot. It can be observed that at tree level the variation of $c_{\beta-\alpha}$ towards larger values results in a decrease of $\kappa_\lambda^{(0)}$, which reaches values close to zero for $c_{\beta-\alpha} \gtrsim 0.1$. Including the one-loop corrections, as shown by the blue solid line, yields a strong increase of $\kappa_\lambda^{(1)}$, with $\kappa_\lambda^{(1)} \gtrsim 5$ for $c_{\beta-\alpha} \gtrsim 0.1$ in this example.

In the right plot we present the corresponding experimental limits and theoretical predictions for the ratio between the 2HDM and SM di-Higgs cross sections, $\mu \equiv \sigma_{2\text{HDM}}/\sigma_{\text{SM}}$, both calculated at LO QCD. The solid (dashed) blue line shows the theory prediction using the one-loop (tree-level) value for κ_λ . The dark red line shows the latest experimental observed limit from non-resonant searches reported by ATLAS [28]. The solid (dashed) line indicates the observed limit for the value of κ_λ that we have calculated at NLO (LO). The corresponding gray line represents the expected limit for κ_λ at NLO (LO). Confronting the experimental limits with the theoretical predictions, a value of $c_{\beta-\alpha}$ is regarded

as excluded if the predicted cross section is larger than the experimentally excluded one. One can see that non-resonant di-Higgs searches would not exclude any value of $c_{\beta-\alpha}$ for the case where $\kappa_\lambda^{(0)}$ is used. As a consequence of the large loop corrections to κ_λ this changes once the one-loop corrections are taken into account. One can see that in this case for the considered example the non-resonant searches exclude a region for large $c_{\beta-\alpha}$ values that is allowed by all other constraints. This underlines the fact that the search for di-Higgs production at the LHC already provides sensitivity to parameter regions of the 2HDM that were unconstrained so far, see also Ref. [27], where scenarios with $c_{\beta-\alpha} = 0$ have been considered.

4.2 Resonant production

We now turn to the interpretation of experimental limits for resonant di-Higgs production in the 2HDM. The resonant limits that have been presented by ATLAS and CMS so far were obtained assuming that only one heavy resonance is realized, neglecting the contributions of the continuum diagrams. This approach is potentially problematic since in any realistic scenario the contributions of the non-resonant diagrams A and C in Fig. 1 will of course always be present in addition to the possible resonant contribution of an additional Higgs boson. The limits obtained by ATLAS and CMS can therefore only be directly applied to scenarios where the impact of the non-resonant diagrams A and C in Fig. 1 is negligible compared to the contribution of the resonant diagram B. Using the 2HDM as a test case for scenarios that have been claimed to be excluded or non-excluded by ATLAS and CMS we will investigate in the following to what extent the assumption made in obtaining the experimental limits is justified.

We note that the assumption of restricting to the resonant contribution implies that the m_{hh} distribution corresponding to the assumed signal will have a peak structure located at $m_{hh} \approx m_H$. This peak structure can potentially be modified by the continuum contributions and by interference effects, where the latter in particular can give rise to peak-dip or dip-peak structures. In the context of assessing the non-resonant contribution arising from the exchange of the detected Higgs boson at 125 GeV (diagram A in Fig. 1) we will analyze the impact of loop corrections to κ_λ .

As a first step, to demonstrate the various possible interference and higher-order effects, we show in Fig. 5 the invariant mass distributions for the benchmark point used in Fig. 2, which is defined in Eq. (14). This benchmark point is allowed by all theoretical and experimental constraints. The blue curves show the pure resonant result, while the red curves correspond to the complete model calculation, including also the non-resonant diagrams and the interference contributions.

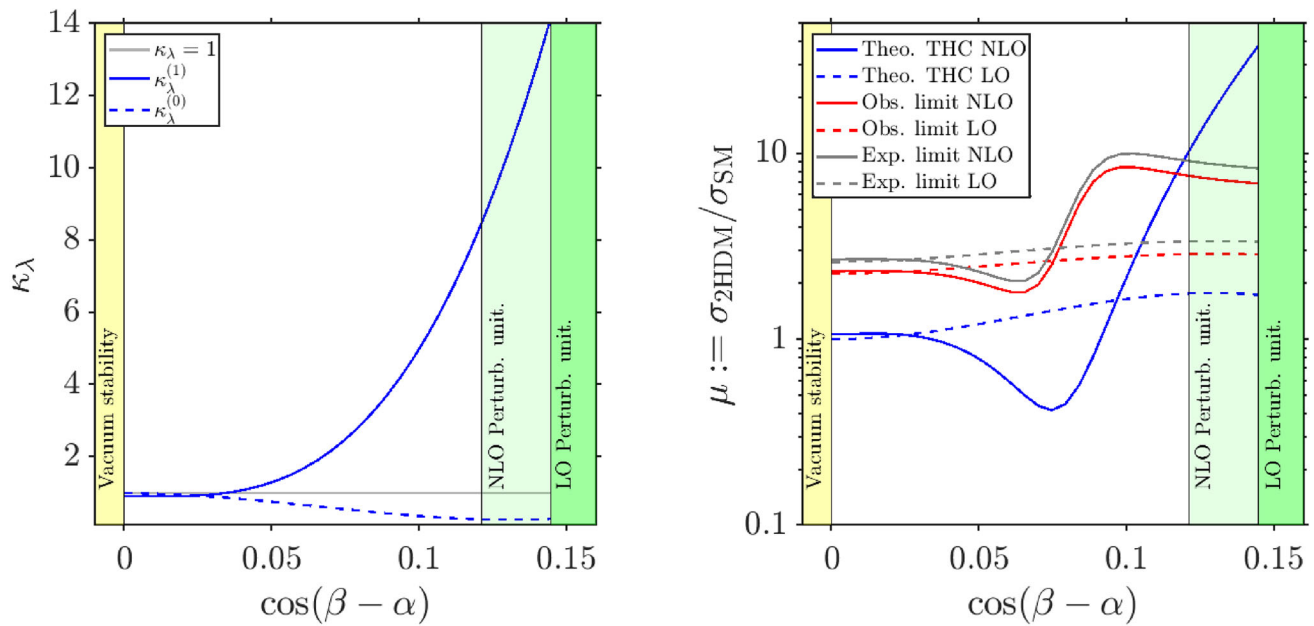


Fig. 4 2HDM type I scenario described in Eq. (20). Left: κ_λ as a function of $c_{\beta-\alpha}$. The gray (blue dashed, blue solid) line shows the result for $\lambda_{\text{SM}}^{(0)}$ ($\lambda_{hh}^{(0)}$, $\lambda_{hhH}^{(1)}$), normalized to $\lambda_{\text{SM}}^{(0)}$. Right: Limits on $\mu \equiv \sigma_{2\text{HDM}}/\sigma_{\text{SM}}$ (each cross section calculated at LO QCD) as function of $c_{\beta-\alpha}$. Red, gray and blue: expected, observed experimental limits

and theory predictions with κ_λ taken at LO (dashed) and NLO (full). In both plots the parameter space excluded by theoretical constraints is indicated by the yellow (vacuum stability), dark green (perturbative unitarity at LO) and light green (perturbative unitarity at NLO) shaded areas

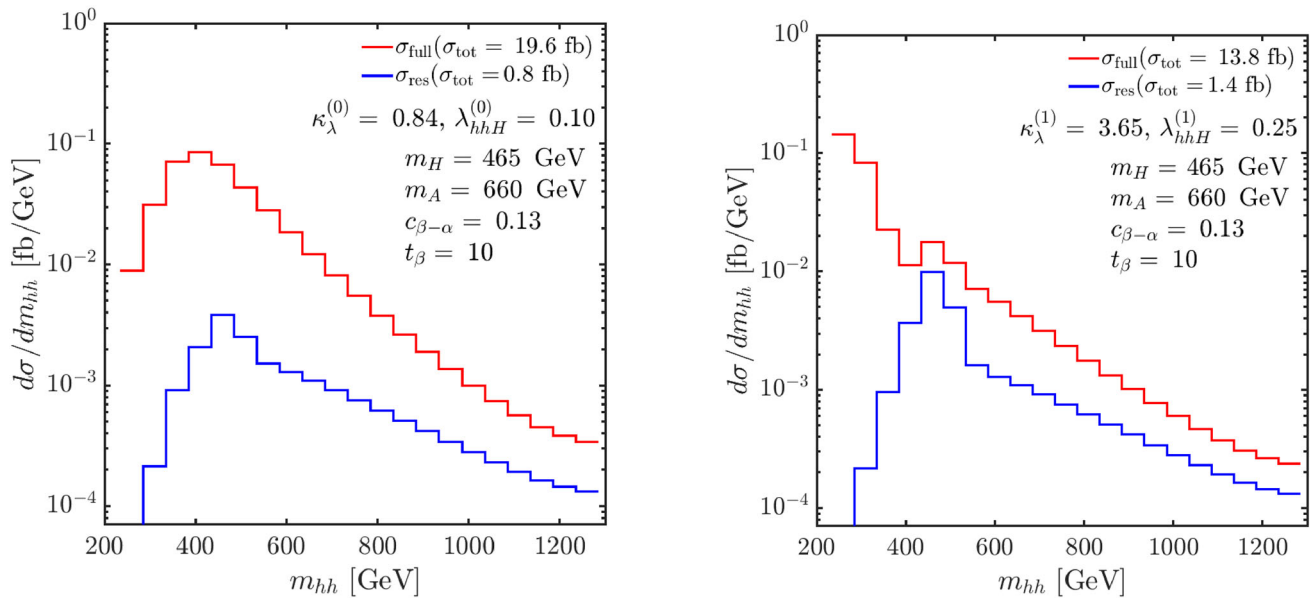


Fig. 5 Invariant mass distribution for the 2HDM type I benchmark point defined in Eq. (14). Left (right) plot: using $\kappa_\lambda^{(0)}$, $\lambda_{hhH}^{(0)}$ ($\kappa_\lambda^{(1)}$, $\lambda_{hhH}^{(1)}$). Red (blue): Complete $\sigma(gg \rightarrow hh)$ prediction (resonance contribution only)

The left (right) plot uses the THCs at LO (NLO). Their values and those of the corresponding total cross sections are specified in the plots. Contrary to the plots in the previous subsections, here we apply a smearing of 15% and a binning in m_{hh} of 50 GeV in order to take into account the limited detector resolution in the experimental analyses, see Ref. [68] for details.

For the case where the tree-level THCs are used, as shown in the left plot of Fig. 5, one can observe that the peak in the m_{hh} distribution given by the pure resonant distribution is broadened substantially over several m_{hh} bins as a consequence of the inclusion of the non-resonant contributions. The effect of the resonance itself is very small, since its contribution to the full result is only about 4%. Furthermore, the “resonance-like” structure of the full result is caused dominantly by the contribution of the continuum diagrams, which peaks slightly above the di-top production threshold (~ 400 GeV), while the resonant contribution (at ~ 465 GeV) in this case is minor and does not appear as a clear resonant structure above the continuum distribution. As can be inferred from the right plot, the inclusion of the NLO contributions to the THCs enhances the pure resonant distribution in this example due to the increased absolute size of $\lambda_{hhH}^{(1)}$ in comparison with $\lambda_{hhH}^{(0)}$, which is also reflected in the result for the total cross section. As indicated by the red curve in the right plot, the combined effect of taking into account non-resonant contributions, interference effects and the NLO corrections to the THCs has a drastic effect on the predicted m_{hh} distribution. Instead of a pronounced peak as it would be expected from the pure resonant contribution, the full result incorporating all relevant contributions gives rise to an m_{hh} distribution that is overall smoothly falling with just a small modulation near $m_{hh} \approx m_H$. Resolving this structure experimentally will clearly be much more challenging than it would be the case if the distribution had the form obtained from restricting to the pure resonant contribution. A striking feature that can be inferred from the plot is the large effect of the non-resonant contributions on the m_{hh} distribution just above the threshold at $m_{hh} \sim 250$ GeV. In this region the differential cross section for the full result differs by several orders of magnitude from the one for the pure resonant contribution. The shape of the differential cross section in this region is also very significantly modified in comparison to the prediction using the THCs at lowest order (red curve in the left plot). As discussed above, the latter large enhancement happens as a result of a change in κ_λ which affects the cancellation between the triangle and box form factors of the continuum diagrams that is present at the m_{hh} threshold at leading order. For $\kappa_\lambda \neq 1$ this cancellation does not take place, giving rise to a large enhancement just above the threshold.

While the benchmark point that we have discussed in Fig. 5 is unexcluded by the non-resonant and resonant

searches, we now turn to two benchmark points that are claimed to be excluded by the existing resonant searches. In Figs. 6 and 7 we show the results for the two benchmark points in the 2HDM type I. For each case we compare the m_{hh} distributions based purely on the resonant diagram, shown in blue, with the one based on the full calculation, shown in red. In the displayed results the NLO results for the THCs have been used (with the values given in the respective plots). Like in the previous plots, all results are shown at LO in QCD. By comparing the predicted distributions based on the full result with the ones based on only the pure resonant contribution we will investigate to what extent the assumption of taking into account only the pure resonant contributions is justified.

The input parameters for the selected benchmark points are defined in Table 1. These points have been obtained as part of a broader scan of the 2HDM parameter space, on which we will report in more detail in a forthcoming publication. We also give the total cross section values calculated with HPAIR for the two benchmark points in Table 2. In column 2 and 3 we show the results of the full calculation at LO and NLO QCD, respectively (confirming the factor of about 2 between them, as mentioned above). In column 4 and 5 we give the corresponding results taking into account only the resonant diagram. The cross section values at LO QCD quoted in the legends of the figures correspond to the integrated curves of Figs. 6 and 7. Column 6 shows the “obs. ratio”, calculated with HiggsTools [71–79]. The obs. ratio is defined as

$$\text{obs. ratio} \equiv \frac{\sigma^{\text{model}}(ggH) \times \text{BR}^{\text{model}}(H \rightarrow hh)}{\sigma^{\text{obs}}(ggH) \times \text{BR}^{\text{obs}}(H \rightarrow hh)}, \quad (21)$$

where the superscript “obs.” refers to the observed experimental limit and “model” refers to the 2HDM. Here, the model cross sections have been calculated at NLO QCD in the Born improved heavy-top limit, using HPAIR. The model branching ratios have been obtained with HDECAY [80, 81], which we modified to include the effective NLO coupling $\lambda_{hhH}^{(1)}$ in the decay width of the heavy Higgs boson into the SM-like Higgs boson pair. These calculated 2HDM cross section and branching ratio values are then provided as inputs for HiggsTools. The definition Eq. (21) implies that the points with an observed ratio larger than 1 are excluded by experimental searches. In view of the assumptions made in the experimental analyses we apply this limit only to the resonant contribution σ^{res} . The benchmark points BP1 (Fig. 6) and BP2 (Fig. 7) are both excluded by the resonant search $pp \rightarrow hh \rightarrow b\bar{b}\tau^+\tau^-$ [82]⁹.

Figure 6 shows the result for the benchmark point BP1, which is claimed to be excluded by resonant di-Higgs searches, but not by non-resonant searches. This point is characterized by significant corrections to κ_λ , corresponding to a parameter region where the one-loop effective coupling

⁹ This search is included in HiggsTools dataset since version v1.6.

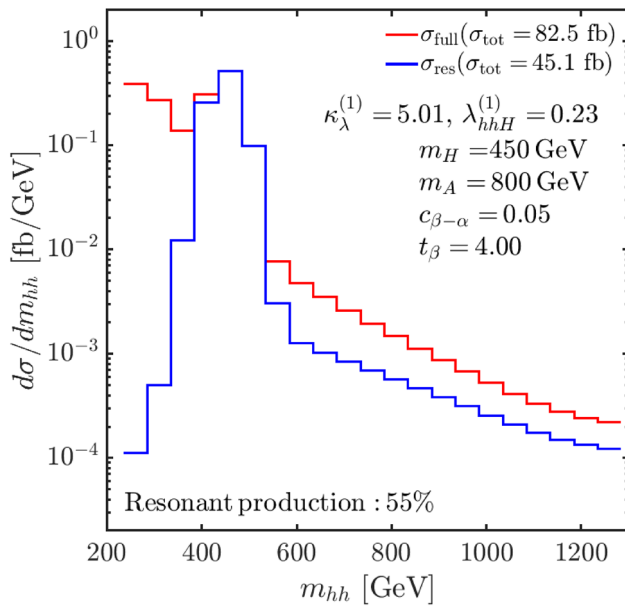


Fig. 6 BP1 (allowed by non-resonant searches, excluded by resonant searches): Invariant mass distribution versus the invariant mass for the full result (red) and the result based on the pure resonant contribution (blue)

approximation is well justified. Specifically, we find

$$\kappa_\lambda^{(0)} = 0.94, \quad \kappa_\lambda^{(1)} = 5.01, \quad \lambda_{hhH}^{(0)} = 0.21 \text{ and } \lambda_{hhH}^{(1)} = 0.23, \quad (22)$$

and

$$\lambda_{hHH}^{(0)} = 0.37, \quad \lambda_{hHH}^{(1)} = -0.06, \\ \lambda_{hAA/hH^\pm H^\mp}^{(0)} = 7.56 \text{ and } \lambda_{hAA/hH^\pm H^\mp}^{(1)} = 0.30. \quad (23)$$

The results given for the total cross sections indicate that the pure resonant contribution amounts to about half of the full result (both at LO and NLO QCD), this is indicated with the percentage of the resonant production contribution in the full process, displayed in the bottom of Fig. 6. Concerning the m_{hh} distributions, one can see that the qualitative features are similar to the right plot of Fig. 5. While the pure resonant contribution shows a pronounced peak, this peak-like structure appears only as a rather small modulation of a smoothly falling distribution in the full result. As in Fig. 5 the cross section just above the hh threshold is enhanced by several orders of magnitude compared to the expectation based on the pure resonant contribution. The peak-like structure in the full result will clearly be much more difficult to resolve experimentally than it would seem to be the case based on the pure resonant contribution. We therefore conclude that the exclusion limits obtained for the resonant di-Higgs searches by ATLAS and CMS may be too optimistic in view of the modifications that occur in the invariant m_{hh} mass distribution

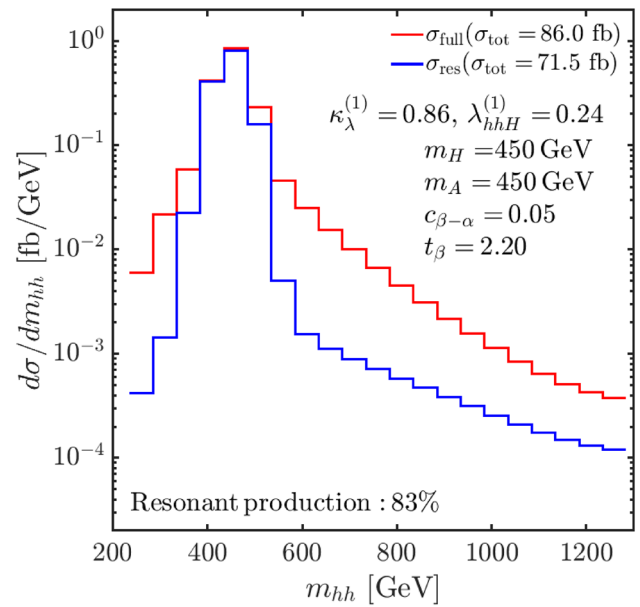


Fig. 7 Same as Fig. 6, but for BP2 (allowed by non-resonant searches, excluded by resonant searches)

upon the inclusion of the SM-like non-resonant contributions that are present in all realistic scenarios and of the relevant interference contributions.

Our second example, BP2, is shown in Fig. 7, and defined by the input values in the second row of Table 1. As BP1, it is claimed to be excluded by resonant di-Higgs searches, but not by the non-resonant ones. Contrary to BP1, the higher-order corrections to the THCs are substantially smaller. We find

$$\kappa_\lambda^{(0)} = 0.96, \quad \kappa_\lambda^{(1)} = 0.86, \quad \lambda_{hhH}^{(0)} = 0.20 \text{ and } \lambda_{hhH}^{(1)} = 0.24, \quad (24)$$

and

$$\lambda_{hHH}^{(0)} = 0.15, \quad \lambda_{hHH}^{(1)} = -0.05, \\ \lambda_{hAA/hH^\pm H^\mp}^{(0)} = 0.12 \text{ and } \\ \lambda_{hAA/hH^\pm H^\mp}^{(1)} = -0.05. \quad (25)$$

For this parameter point the m_{hh} distribution based on the pure resonant contribution and on the full result are more similar than in the previous example, and the pure resonant contribution amounts to about 83% of the full cross section. However, still a substantial broadening of the peak by the inclusion of the non-resonant diagrams can be observed. Similarly to BP1, we therefore conclude that the exclusion limits obtained for the resonant di-Higgs searches by ATLAS and CMS are possibly too optimistic in view of the m_{hh} modifications due to the inclusion of all the relevant contributions in a realistic scenario.

Table 1 Input parameters for the selected benchmark points. Masses are given in GeV

	t_β	$c_{\beta-\alpha}$ ($s_{\beta-\alpha} > 0$)	m_H	$m_A = m_{H^\pm}$	m_{12}^2
BP1	4.0	0.05	450	800	$m_{12}^2 = m_H^2 c_\alpha^2 / t_\beta$
BP2	2.2	0.05	450	450	$m_{12}^2 = m_H^2 c_\alpha^2 / t_\beta$

Table 2 Higgs pair production cross sections $\sigma(gg \rightarrow hh)$ [fb] and the resonant contribution only (σ^{res}), computed with HPAIR at LO and NLO QCD in the Born improved heavy-top limit for the total cross section, respectively; “obs. ratio” obtained with HiggsTools (see text)

	σ (LO QCD)	σ (NLO QCD)	σ^{res} (LO QCD)	σ^{res} (NLO QCD)	obs. ratio
BP1	82.53	165.89	45.06	89.23	1.8
BP2	85.95	169.03	71.51	140.77	2.9

Our discussion shows that the sensitivity of the resonant di-Higgs searches by ATLAS and CMS has already reached a level of sensitivity that strongly motivates to go beyond the assumption of restricting to the pure resonant contribution in deriving the experimental limits. A dedicated joint effort of experiment and theory would be desirable to define an appropriate framework in which the experimental limits should be presented in the future. In particular, the non-resonant contributions should be included in the signal model, and the possibility of interference effects between the resonant and non-resonant contributions should be incorporated. This will require an extension of the analysis setup involving additional parameters.

5 Conclusions

The determination of the trilinear Higgs self-coupling as a first step towards elucidating the shape of the Higgs potential will be a prime goal of particle physics at the LHC and beyond. The current bounds on the trilinear Higgs self-coupling leave significant room for deviations of this coupling from the SM value. Such deviations in κ_λ can occur in simple extensions of the SM such as the 2HDM, where they arise in particular from loop corrections involving additional Higgs bosons. While we have used the 2HDM as theoretical framework in our analysis, our qualitative results are applicable to a wide class of models of extended Higgs sectors.

In our analysis we have emphasized the need to compare the experimental results for di-Higgs production with precise theoretical predictions, in particular including electroweak corrections besides QCD corrections, as they may lead to large effects in models with extended scalar sectors. Starting with an investigation of the experimental bounds that have been obtained from non-resonant di-Higgs production, we have investigated the impact of the loop contributions to κ_λ . Our results underline that, once the radiative corrections to

the Higgs self-interactions are taken into account, the experimental bounds from the search for di-Higgs production at the LHC already provide sensitivity to parameter regions of the 2HDM that were unconstrained so far based on all other existing experimental and theoretical limits.

We have then analyzed in detail the case where the di-Higgs production process receives a contribution from the resonant production of an additional neutral Higgs boson. The limits from those resonant searches that have been presented by ATLAS and CMS so far were obtained assuming a signal model consisting only of the resonant contribution, while the non-resonant SM-like contributions involving the s -channel exchange of the detected Higgs boson at 125 GeV as well as the box-type top-quark loop contribution have been neglected. Accordingly, the limits obtained by ATLAS and CMS can only be directly applied to scenarios where the impact of the non-resonant contributions is negligible compared to the pure resonant contribution. Using the 2HDM as a test case we have compared the full result for the m_{hh} invariant mass distribution, consisting of both the resonant and the non-resonant contributions as well as the interference effects and taking into account the loop corrections to the trilinear Higgs self-couplings λ_{hhh} and λ_{hhH} , with the pure resonant contribution as used by ATLAS and CMS. In order to take into account the limited detector resolution in the experimental analyses we have applied a smearing of 15% and a binning in m_{hh} of 50 GeV in our phenomenological study.

While the assumption of restricting to the pure resonant contribution made by ATLAS and CMS implies that the m_{hh} distribution corresponding to the assumed signal has a peak structure located at $m_{hh} \approx m_H$, the non-resonant contributions and the interference effects can modify this behavior. Indeed, we have found that the distributions based on the prediction arising from the full result can be significantly distorted as compared to the distribution that would be expected from the pure resonant contribution. Instead of a pronounced peak as it would be expected from the pure resonant contribu-

tion, we have demonstrated that the full result incorporating all relevant contributions can give rise to an m_{hh} distribution that is overall smoothly falling with just a small modulation near $m_{hh} \approx m_H$. The task to experimentally resolve this structure is clearly much more difficult than it would be the case if the distribution had the form as expected from the pure resonant contribution. We have pointed out the importance of the loop contributions to the trilinear Higgs self-couplings in this context. A striking feature related to the loop corrections to κ_λ is a large effect on the differential cross section just above the hh threshold. It arises because a large cancellation between the triangle and box form factors of the continuum diagrams that is present at the m_{hh} threshold at leading order no longer occurs upon the inclusion of the loop corrections.

In our numerical analysis we have specifically investigated examples of parameter points that would be classified as excluded according to the existing resonant searches and assessed to what extent the assumption of neglecting the non-resonant contributions made in obtaining the experimental limits is justified. Also in these cases we have found significant distortions of the distributions compared to the expectation from the pure resonant contribution. This implies that the exclusion limits obtained for the resonant di-Higgs searches by ATLAS and CMS may be too optimistic in view of the modifications that occur in the invariant m_{hh} mass distribution in realistic scenarios upon the inclusion of all the relevant contributions.

The results obtained in our paper indicate that the resonant di-Higgs searches carried out by ATLAS and CMS have meanwhile reached a level of sensitivity that strongly motivates to define an appropriate framework in which the experimental limits should be presented in the future. Avoiding the assumption of restricting to the pure resonant contribution in deriving the experimental limits, such a framework should make it possible to directly compare the experimental results with theoretical predictions in extended Higgs sectors. A dedicated joint effort of experiment and theory would seem to be desirable in this context.

Acknowledgements We thank Francisco Arco, Johannes Braathen and Michael Spira for useful discussions. The work of S.H. has received financial support from the grant PID2019-110058GB-C21 funded by MCIN/AEI/10.13039/501100011033 and by “ERDF A way of making Europe”, and in part by the grant IFT Centro de Excelencia Severo Ochoa CEX2020-001007-S funded by MCIN/AEI/10.13039/501100011033. S.H. also acknowledges support from Grant PID2022-142545NB-C21 funded by MCIN/AEI/10.13039/501100011033/FEDER, UE. The work of M.M. has been supported by the BMBF-Project 05H21VKCCA. K.R. and G.W. acknowledge support by the Deutsche Forschungsgemeinschaft (DFG, German Research Foundation) under Germany’s Excellence Strategy – EXC 2121 “Quantum Universe” – 390833306. This work has been partially funded by the Deutsche Forschungsgemeinschaft (DFG, German Research Foundation) – 491245950.

Data Availability Statement This manuscript has no associated data. [Authors’ comment: Data sharing not applicable to this article as no datasets were generated or analysed during the current study.]

Code Availability Statement This manuscript has no associated code/software. [Authors’ comment: Code/Software sharing not applicable to this article as no code/software was generated or analysed during the current study.]

Open Access This article is licensed under a Creative Commons Attribution 4.0 International License, which permits use, sharing, adaptation, distribution and reproduction in any medium or format, as long as you give appropriate credit to the original author(s) and the source, provide a link to the Creative Commons licence, and indicate if changes were made. The images or other third party material in this article are included in the article’s Creative Commons licence, unless indicated otherwise in a credit line to the material. If material is not included in the article’s Creative Commons licence and your intended use is not permitted by statutory regulation or exceeds the permitted use, you will need to obtain permission directly from the copyright holder. To view a copy of this licence, visit <http://creativecommons.org/licenses/by/4.0/>. Funded by SCOAP³.

References

1. ATLAS Collaboration, Observation of a new particle in the search for the Standard Model Higgs boson with the ATLAS detector at the LHC. *Phys. Lett. B* **716**, 1 (2012). <https://doi.org/10.1016/j.physletb.2012.08.020>. arXiv:1207.7214
2. CMS Collaboration, Observation of a new boson at a mass of 125 GeV with the CMS experiment at the LHC. *Phys. Lett. B* **716**, 30 (2012). <https://doi.org/10.1016/j.physletb.2012.08.021>. arXiv:1207.7235
3. ATLAS, CMS Collaboration, Measurements of the Higgs boson production and decay rates and constraints on its couplings from a combined ATLAS and CMS analysis of the LHC pp collision data at $\sqrt{s} = 7$ and 8 TeV. *JHEP* **08**, 045 (2016). [https://doi.org/10.1007/JHEP08\(2016\)045](https://doi.org/10.1007/JHEP08(2016)045). arXiv:1606.02266
4. CMS Collaboration, A portrait of the Higgs boson by the CMS experiment ten years after the discovery. *Nature* **607**, 60 (2022). <https://doi.org/10.1038/s41586-022-04892-x>. arXiv:2207.00043
5. ATLAS Collaboration, A detailed map of Higgs boson interactions by the ATLAS experiment ten years after the discovery. *Nature* **607**, 52 (2022). <https://doi.org/10.1038/s41586-022-04893-w>. arXiv:2207.00092
6. A. Djouadi, W. Kilian, M. Muhlleitner, P.M. Zerwas, Testing Higgs selfcouplings at e+ e- linear colliders. *Eur. Phys. J. C* **10**, 27 (1999). <https://doi.org/10.1007/s100529900082>. arXiv: hep-ph/9903229
7. A. Djouadi, W. Kilian, M. Muhlleitner, P.M. Zerwas, Production of neutral Higgs boson pairs at LHC. *Eur. Phys. J. C* **10**, 45 (1999). <https://doi.org/10.1007/s100529900083>. arXiv: hep-ph/9904287
8. WMAP Collaboration, Nine-Year Wilkinson Microwave Anisotropy Probe (WMAP) observations: final maps and results. *Astrophys. J. Suppl.* **208**, 20 (2013). <https://doi.org/10.1088/0067-0049/208/2/20>. arXiv:1212.5225
9. V.A. Kuzmin, V.A. Rubakov, M.E. Shaposhnikov, On the anomalous electroweak baryon number nonconservation in the early universe. *Phys. Lett. B* **155**, 36 (1985). [https://doi.org/10.1016/0370-2693\(85\)91028-7](https://doi.org/10.1016/0370-2693(85)91028-7)
10. A.G. Cohen, D.B. Kaplan, A.E. Nelson, Baryogenesis at the weak phase transition. *Nucl. Phys. B* **349**, 727 (1991). [https://doi.org/10.1016/0550-3213\(91\)90395-E](https://doi.org/10.1016/0550-3213(91)90395-E)

11. A.G. Cohen, D.B. Kaplan, A.E. Nelson, Progress in electroweak baryogenesis. *Annu. Rev. Nucl. Part. Sci.* **43**, 27 (1993). <https://doi.org/10.1146/annurev.ns.43.120193.000331>. [arXiv:hep-ph/9302210](https://arxiv.org/abs/hep-ph/9302210)
12. M. Quiros, Field theory at finite temperature and phase transitions. *Helv. Phys. Acta* **67**, 451 (1994)
13. V.A. Rubakov, M.E. Shaposhnikov, Electroweak baryon number nonconservation in the early universe and in high-energy collisions. *Usp. Fiz. Nauk* **166**, 493 (1996). <https://doi.org/10.1070/PU1996v039n05ABEH000145>. [arXiv:hep-ph/9603208](https://arxiv.org/abs/hep-ph/9603208)
14. K. Funakubo, CP violation and baryogenesis at the electroweak phase transition. *Prog. Theor. Phys.* **96**, 475 (1996). <https://doi.org/10.1143/PTP.96.475>. [arXiv:hep-ph/9608358](https://arxiv.org/abs/hep-ph/9608358)
15. M. Trodden, Electroweak baryogenesis. *Rev. Mod. Phys.* **71**, 1463 (1999). <https://doi.org/10.1103/RevModPhys.71.1463>. [arXiv:hep-ph/9803479](https://arxiv.org/abs/hep-ph/9803479)
16. W. Bernreuther, CP violation and baryogenesis. *Lect. Notes Phys.* **591**, 237 (2002). [arXiv:hep-ph/0205279](https://arxiv.org/abs/hep-ph/0205279)
17. D.E. Morrissey, M.J. Ramsey-Musolf, Electroweak baryogenesis. *New J. Phys.* **14**, 125003 (2012). <https://doi.org/10.1088/1367-2630/14/12/125003>. [arXiv:1206.2942](https://arxiv.org/abs/1206.2942)
18. A.D. Sakharov, Violation of CP invariance, C asymmetry, and baryon asymmetry of the universe. *Pisma Zh. Eksp. Teor. Fiz.* **5**, 32 (1967). <https://doi.org/10.1070/PU1991v034n05ABEH002497>
19. S. Kanemura, Y. Okada, E. Senaha, Electroweak baryogenesis and quantum corrections to the triple Higgs boson coupling. *Phys. Lett. B* **606**, 361 (2005). <https://doi.org/10.1016/j.physletb.2004.12.004>. [arXiv:hep-ph/0411354](https://arxiv.org/abs/hep-ph/0411354)
20. A. Noble, M. Perelstein, Higgs self-coupling as a probe of electroweak phase transition. *Phys. Rev. D* **78**, 063518 (2008). <https://doi.org/10.1103/PhysRevD.78.063518>. [arXiv:0711.3018](https://arxiv.org/abs/0711.3018)
21. P. Huang, A. Joglekar, B. Li, C.E.M. Wagner, Probing the electroweak phase transition at the LHC. *Phys. Rev. D* **93**, 055049 (2016). <https://doi.org/10.1103/PhysRevD.93.055049>. [arXiv:1512.00068](https://arxiv.org/abs/1512.00068)
22. M. Reichert, A. Eichhorn, H. Gies, J.M. Pawłowski, T. Plehn, M.M. Scherer, Probing baryogenesis through the Higgs boson self-coupling. *Phys. Rev. D* **97**, 075008 (2018). <https://doi.org/10.1103/PhysRevD.97.075008>. [arXiv:1711.00019](https://arxiv.org/abs/1711.00019)
23. C. Grojean, G. Servant, J.D. Wells, First-order electroweak phase transition in the standard model with a low cutoff. *Phys. Rev. D* **71**, 036001 (2005). <https://doi.org/10.1103/PhysRevD.71.036001>. [arXiv:hep-ph/0407019](https://arxiv.org/abs/hep-ph/0407019)
24. P. Basler, M. Mühlleitner, J. Wittbrodt, The CP-violating 2HDM in light of a strong first order electroweak phase transition and implications for Higgs pair production. *JHEP* **03**, 061 (2018). [https://doi.org/10.1007/JHEP03\(2018\)061](https://doi.org/10.1007/JHEP03(2018)061). [arXiv:1711.04097](https://arxiv.org/abs/1711.04097)
25. P. Basler, M. Mühlleitner, J. Müller, Electroweak phase transition in non-minimal Higgs sectors. *JHEP* **05**, 016 (2020). [https://doi.org/10.1007/JHEP05\(2020\)016](https://doi.org/10.1007/JHEP05(2020)016). [arXiv:1912.10477](https://arxiv.org/abs/1912.10477)
26. S. Kanemura, Y. Okada, E. Senaha, C.P. Yuan, Higgs coupling constants as a probe of new physics. *Phys. Rev. D* **70**, 115002 (2004). <https://doi.org/10.1103/PhysRevD.70.115002>. [arXiv:hep-ph/0408364](https://arxiv.org/abs/hep-ph/0408364)
27. H. Bahl, J. Braathen, G. Weiglein, New constraints on extended Higgs sectors from the trilinear Higgs coupling. *Phys. Rev. Lett.* **129**, 231802 (2022). <https://doi.org/10.1103/PhysRevLett.129.231802>. [arXiv:2202.03453](https://arxiv.org/abs/2202.03453)
28. ATLAS Collaboration, Constraints on the Higgs boson self-coupling from single- and double-Higgs production with the ATLAS detector using pp collisions at $\sqrt{s}=13$ TeV. *Phys. Lett. B* **843**, 137745 (2023). <https://doi.org/10.1016/j.physletb.2023.137745>. [arXiv:2211.01216](https://arxiv.org/abs/2211.01216)
29. J. de Blas et al., Higgs boson studies at future particle colliders. *JHEP* **01**, 139 (2020). [https://doi.org/10.1007/JHEP01\(2020\)139](https://doi.org/10.1007/JHEP01(2020)139). [arXiv:1905.03764](https://arxiv.org/abs/1905.03764)
30. ATLAS Collaboration, HL-LHC prospects for the measurement of Higgs boson pair production in the $b\bar{b}b\bar{b}$ final state and combination with the $b\bar{b}\gamma\gamma$ and $b\bar{b}\tau^+\tau^-$ final states at the ATLAS experiment
31. T. Lee, A theory of spontaneous t violation. *Phys. Rev. D* **8**, 1226 (1973)
32. J.F. Gunion, H.E. Haber, G.L. Kane, S. Dawson, *The Higgs Hunter's Guide*, vol. 80 (2000)
33. M. Aoki, S. Kanemura, K. Tsumura, K. Yagyu, Models of Yukawa interaction in the two Higgs doublet model, and their collider phenomenology. *Phys. Rev. D* **80**, 015017 (2009). <https://doi.org/10.1103/PhysRevD.80.015017>. [arXiv:0902.4665](https://arxiv.org/abs/0902.4665)
34. G.C. Branco, P.M. Ferreira, L. Lavoura, M.N. Rebelo, M. Sher, J.P. Silva, Theory and phenomenology of two-Higgs-doublet models. *Phys. Rep.* **516**, 1 (2012). <https://doi.org/10.1016/j.physrep.2012.02.002>. [arXiv:1106.0034](https://arxiv.org/abs/1106.0034)
35. J.F. Gunion, H.E. Haber, The CP conserving two Higgs doublet model: the approach to the decoupling limit. *Phys. Rev. D* **67**, 075019 (2003). <https://doi.org/10.1103/PhysRevD.67.075019>. [arXiv:hep-ph/0207010](https://arxiv.org/abs/hep-ph/0207010)
36. F. Arco, S. Heinemeyer, M.J. Herrero, Exploring sizable triple Higgs couplings in the 2HDM. *Eur. Phys. J. C* **80**, 884 (2020). <https://doi.org/10.1140/epjc/s10052-020-8406-8>. [arXiv:2005.10576](https://arxiv.org/abs/2005.10576)
37. H. Abouabid, A. Arhrib, D. Azevedo, J.E. Falaki, P.M. Ferreira, M. Mühlleitner et al., Benchmarking di-Higgs production in various extended Higgs sector models. *JHEP* **09**, 011 (2022). [https://doi.org/10.1007/JHEP09\(2022\)011](https://doi.org/10.1007/JHEP09(2022)011). [arXiv:2112.12515](https://arxiv.org/abs/2112.12515)
38. F. Arco, S. Heinemeyer, M.J. Herrero, Triple Higgs couplings in the 2HDM: the complete picture. *Eur. Phys. J. C* **82**, 536 (2022). <https://doi.org/10.1140/epjc/s10052-022-10485-9>. [arXiv:2203.12684](https://arxiv.org/abs/2203.12684)
39. S. Kanemura, S. Kiyoura, Y. Okada, E. Senaha, C.P. Yuan, New physics effect on the Higgs selfcoupling. *Phys. Lett. B* **558**, 157 (2003). [https://doi.org/10.1016/S0370-2693\(03\)00268-5](https://doi.org/10.1016/S0370-2693(03)00268-5). [arXiv:hep-ph/0211308](https://arxiv.org/abs/hep-ph/0211308)
40. J. Braathen, S. Kanemura, On two-loop corrections to the Higgs trilinear coupling in models with extended scalar sectors. *Phys. Lett. B* **796**, 38 (2019). <https://doi.org/10.1016/j.physletb.2019.07.021>. [arXiv:1903.05417](https://arxiv.org/abs/1903.05417)
41. J. Braathen, S. Kanemura, Leading two-loop corrections to the Higgs boson self-couplings in models with extended scalar sectors. *Eur. Phys. J. C* **80**, 227 (2020). <https://doi.org/10.1140/epjc/s10052-020-7723-2>. [arXiv:1911.11507](https://arxiv.org/abs/1911.11507)
42. P. Basler, M. Mühlleitner, BSMPT (Beyond the Standard Model Phase Transitions): a tool for the electroweak phase transition in extended Higgs sectors. *Comput. Phys. Commun.* **237**, 62 (2019). <https://doi.org/10.1016/j.cpc.2018.11.006>. [arXiv:1803.02846](https://arxiv.org/abs/1803.02846)
43. P. Basler, M. Mühlleitner, J. Müller, BSMPT v2 a tool for the electroweak phase transition and the baryon asymmetry of the universe in extended Higgs Sectors. *Comput. Phys. Commun.* **269**, 108124 (2021). <https://doi.org/10.1016/j.cpc.2021.108124>. [arXiv:2007.01725](https://arxiv.org/abs/2007.01725)
44. E.J. Weinberg, Radiative corrections as the origin of spontaneous symmetry breaking, Ph.D. thesis (Harvard University, 1973). [arXiv:hep-th/0507214](https://arxiv.org/abs/hep-th/0507214)
45. S.R. Coleman, E.J. Weinberg, Radiative corrections as the origin of spontaneous symmetry breaking. *Phys. Rev. D* **7**, 1888 (1973). <https://doi.org/10.1103/PhysRevD.7.1888>
46. H. Bahl, J. Braathen, M. Gabelmann, G. Weiglein, anyH3: precise predictions for the trilinear Higgs coupling in the Standard Model and beyond. *Eur. Phys. J. C* **83**, 1156 (2023). <https://doi.org/10.1140/epjc/s10052-023-12173-8>. [arXiv:2305.03015](https://arxiv.org/abs/2305.03015)
47. M. Grazzini, G. Heinrich, S. Jones, S. Kallweit, M. Kerner, J.M. Lindert et al., Higgs boson pair production at NNLO with top quark mass effects. *JHEP* **05**, 059 (2018). [https://doi.org/10.1007/JHEP05\(2018\)059](https://doi.org/10.1007/JHEP05(2018)059). [arXiv:1803.02463](https://arxiv.org/abs/1803.02463)

48. J. Baglio, F. Campanario, S. Glaus, M. Mühlleitner, J. Ronca, M. Spira, $gg \rightarrow HH$: combined uncertainties. *Phys. Rev. D* **103**, 056002 (2021). <https://doi.org/10.1103/PhysRevD.103.056002>. [arXiv:2008.11626](https://arxiv.org/abs/2008.11626)
49. D. de Florian, J. Mazzitelli, Higgs boson pair production at next-to-next-to-leading order in QCD. *Phys. Rev. Lett.* **111**, 201801 (2013). <https://doi.org/10.1103/PhysRevLett.111.201801>. [arXiv:1309.6594](https://arxiv.org/abs/1309.6594)
50. J. Grigo, K. Melnikov, M. Steinhauser, Virtual corrections to Higgs boson pair production in the large top quark mass limit. *Nucl. Phys. B* **888**, 17 (2014). <https://doi.org/10.1016/j.nuclphysb.2014.09.003>. [arXiv:1408.2422](https://arxiv.org/abs/1408.2422)
51. J. Davies, F. Herren, G. Mishima, M. Steinhauser, Real corrections to Higgs boson pair production at NNLO in the large top quark mass limit. *JHEP* **01**, 049 (2022). [https://doi.org/10.1007/JHEP01\(2022\)049](https://doi.org/10.1007/JHEP01(2022)049). [arXiv:2110.03697](https://arxiv.org/abs/2110.03697)
52. S. Borowka, N. Greiner, G. Heinrich, S.P. Jones, M. Kerner, J. Schlenk et al., Higgs boson pair production in gluon fusion at next-to-leading order with full top-quark mass dependence. *Phys. Rev. Lett.* **117**, 012001 (2016). <https://doi.org/10.1103/PhysRevLett.117.079901>. [arXiv:1604.06447](https://arxiv.org/abs/1604.06447)
53. S. Borowka, N. Greiner, G. Heinrich, S.P. Jones, M. Kerner, J. Schlenk et al., Full top quark mass dependence in Higgs boson pair production at NLO. *JHEP* **10**, 107 (2016). [https://doi.org/10.1007/JHEP10\(2016\)107](https://doi.org/10.1007/JHEP10(2016)107). [arXiv:1608.04798](https://arxiv.org/abs/1608.04798)
54. J. Baglio, F. Campanario, S. Glaus, M. Mühlleitner, M. Spira, J. Streicher, Gluon fusion into Higgs pairs at NLO QCD and the top mass scheme. *Eur. Phys. J. C* **79**, 459 (2019). <https://doi.org/10.1140/epjc/s10052-019-6973-3>. [arXiv:1811.05692](https://arxiv.org/abs/1811.05692)
55. J. Baglio, F. Campanario, S. Glaus, M. Mühlleitner, J. Ronca, M. Spira et al., Higgs-pair production via gluon fusion at hadron colliders: NLO QCD corrections. *JHEP* **04**, 181 (2020). [https://doi.org/10.1007/JHEP04\(2020\)181](https://doi.org/10.1007/JHEP04(2020)181). [arXiv:2003.03227](https://arxiv.org/abs/2003.03227)
56. M. Mühlleitner, J. Schlenk, M. Spira, Top-Yukawa-induced corrections to Higgs pair production. *JHEP* **10**, 185 (2022). [https://doi.org/10.1007/JHEP10\(2022\)185](https://doi.org/10.1007/JHEP10(2022)185). [arXiv:2207.02524](https://arxiv.org/abs/2207.02524)
57. D.T. Nhung, M. Mühlleitner, J. Streicher, K. Walz, Higher order corrections to the trilinear Higgs self-couplings in the real NMSSM. *JHEP* **11**, 181 (2013). [https://doi.org/10.1007/JHEP11\(2013\)181](https://doi.org/10.1007/JHEP11(2013)181). [arXiv:1306.3926](https://arxiv.org/abs/1306.3926)
58. C. Borschensky, T.N. Dao, M. Gabelmann, M. Mühlleitner, H. Rzehak, The trilinear Higgs self-couplings at $\mathcal{O}(\alpha_t^2)$ in the CP-violating NMSSM. *Eur. Phys. J. C* **83**, 118 (2023). <https://doi.org/10.1140/epjc/s10052-023-11215-5>. [arXiv:2210.02104](https://arxiv.org/abs/2210.02104)
59. J. Davies, G. Mishima, K. Schönwald, M. Steinhauser, H. Zhang, Higgs boson contribution to the leading two-loop Yukawa corrections to $gg \rightarrow HH$. *JHEP* **08**, 259 (2022). [https://doi.org/10.1007/JHEP08\(2022\)259](https://doi.org/10.1007/JHEP08(2022)259). [arXiv:2207.02587](https://arxiv.org/abs/2207.02587)
60. J. Davies, K. Schönwald, M. Steinhauser, H. Zhang, Next-to-leading order electroweak corrections to $gg \rightarrow HH$ and $gg \rightarrow gH$ in the large- m_t limit. *JHEP* **10**, 033 (2023). [https://doi.org/10.1007/JHEP10\(2023\)033](https://doi.org/10.1007/JHEP10(2023)033). [arXiv:2308.01355](https://arxiv.org/abs/2308.01355)
61. H.-Y. Bi, L.-H. Huang, R.-J. Huang, Y.-Q. Ma, H.-M. Yu, Electroweak corrections to double Higgs production at the LHC. [arXiv:2311.16963](https://arxiv.org/abs/2311.16963)
62. T. Plehn, M. Spira, P.M. Zerwas, Pair production of neutral Higgs particles in gluon-gluon collisions. *Nucl. Phys. B* **479**, 46 (1996). [https://doi.org/10.1016/0550-3213\(96\)00418-X](https://doi.org/10.1016/0550-3213(96)00418-X). [arXiv:hep-ph/9603205](https://arxiv.org/abs/hep-ph/9603205)
63. S. Dawson, S. Dittmaier, M. Spira, Neutral Higgs boson pair production at hadron colliders: QCD corrections. *Phys. Rev. D* **58**, 115012 (1998). <https://doi.org/10.1103/PhysRevD.58.115012>. [arXiv:hep-ph/9805244](https://arxiv.org/abs/hep-ph/9805244)
64. R. Grober, M. Mühlleitner, M. Spira, Higgs pair production at NLO QCD for CP-violating Higgs sectors. *Nucl. Phys. B* **925**, 1 (2017). <https://doi.org/10.1016/j.nuclphysb.2017.10.002>. [arXiv:1705.05314](https://arxiv.org/abs/1705.05314)
65. J. Baglio, F. Campanario, S. Glaus, M. Mühlleitner, J. Ronca, M. Spira, Full NLO QCD predictions for Higgs-pair production in the 2-Higgs-doublet model. *Eur. Phys. J. C* **83**, 826 (2023). <https://doi.org/10.1140/epjc/s10052-023-11957-2>. [arXiv:2303.05409](https://arxiv.org/abs/2303.05409)
66. S. Dulat, T.-J. Hou, J. Gao, M. Guzzi, J. Huston, P. Nadolsky et al., New parton distribution functions from a global analysis of quantum chromodynamics. *Phys. Rev. D* **93**, 033006 (2016). <https://doi.org/10.1103/PhysRevD.93.033006>. [arXiv:1506.07443](https://arxiv.org/abs/1506.07443)
67. G. Buchalla, M. Capozzi, A. Celis, G. Heinrich, L. Scyboz, Higgs boson pair production in non-linear Effective Field Theory with full m_t -dependence at NLO QCD. *JHEP* **09**, 057 (2018). [https://doi.org/10.1007/JHEP09\(2018\)057](https://doi.org/10.1007/JHEP09(2018)057). [arXiv:1806.05162](https://arxiv.org/abs/1806.05162)
68. F. Arco, S. Heinemeyer, M. Mühlleitner, K. Radchenko, Sensitivity to triple Higgs couplings via di-Higgs production in the 2HDM at the (HL-)LHC. *Eur. Phys. J. C* **83**, 1019 (2023). <https://doi.org/10.1140/epjc/s10052-023-12193-4>. [arXiv:2212.11242](https://arxiv.org/abs/2212.11242)
69. M. Cepeda et al., Report from Working Group 2: Higgs Physics at the HL-LHC and HE-LHC. CERN Yellow Rep. Monogr. **7**, 221 (2019). <https://doi.org/10.23731/CYRM-2019-007.221>. [arXiv:1902.00134](https://arxiv.org/abs/1902.00134)
70. T. Biekötter, S. Heinemeyer, J.M. No, K. Radchenko, M.O.O. Romacho, G. Weiglein, First shot of the smoking gun: probing the electroweak phase transition in the 2HDM with novel searches for $A \rightarrow ZH$ in $\ell^+ \ell^- t \bar{t}$ and $\nu \nu b \bar{b}$ final states. *JHEP* **01**, 107 (2024). [https://doi.org/10.1007/JHEP01\(2024\)107](https://doi.org/10.1007/JHEP01(2024)107). [arXiv:2309.17431](https://arxiv.org/abs/2309.17431)
71. H. Bahl, T. Biekötter, S. Heinemeyer, C. Li, S. Paasch, G. Weiglein et al., HiggsTools: BSM scalar phenomenology with new versions of HiggsBounds and HiggsSignals. *Comput. Phys. Commun.* **291**, 108803 (2023). <https://doi.org/10.1016/j.cpc.2023.108803>. [arXiv:2210.09332](https://arxiv.org/abs/2210.09332)
72. P. Bechtle, O. Brein, S. Heinemeyer, G. Weiglein, K.E. Williams, HiggsBounds: confronting arbitrary Higgs sectors with exclusion bounds from LEP and the Tevatron. *Comput. Phys. Commun.* **181**, 138 (2010). <https://doi.org/10.1016/j.cpc.2009.09.003>. [arXiv:0811.4169](https://arxiv.org/abs/0811.4169)
73. P. Bechtle, O. Brein, S. Heinemeyer, G. Weiglein, K.E. Williams, HiggsBounds 2.0.0: confronting neutral and charged Higgs sector predictions with exclusion bounds from LEP and the Tevatron. *Comput. Phys. Commun.* **182**, 2605 (2011). <https://doi.org/10.1016/j.cpc.2011.07.015>. [arXiv:1102.1898](https://arxiv.org/abs/1102.1898)
74. P. Bechtle, O. Brein, S. Heinemeyer, O. Stål, T. Stefaniak, G. Weiglein et al., HiggsBounds – 4: improved tests of extended Higgs sectors against exclusion bounds from LEP, the Tevatron and the LHC. *Eur. Phys. J. C* **74**, 2693 (2014). <https://doi.org/10.1140/epjc/s10052-013-2693-2>. [arXiv:1311.0055](https://arxiv.org/abs/1311.0055)
75. P. Bechtle, S. Heinemeyer, O. Stål, T. Stefaniak, G. Weiglein, Applying exclusion likelihoods from LHC searches to extended Higgs sectors. *Eur. Phys. J. C* **75**, 421 (2015). <https://doi.org/10.1140/epjc/s10052-015-3650-z>. [arXiv:1507.06706](https://arxiv.org/abs/1507.06706)
76. P. Bechtle, D. Dercks, S. Heinemeyer, T. Klingl, T. Stefaniak, G. Weiglein et al., HiggsBounds-5: testing Higgs sectors in the LHC 13 TeV era. *Eur. Phys. J. C* **80**, 1211 (2020). <https://doi.org/10.1140/epjc/s10052-020-08557-9>. [arXiv:2006.06007](https://arxiv.org/abs/2006.06007)
77. P. Bechtle, S. Heinemeyer, O. Stål, T. Stefaniak, G. Weiglein, HiggsSignals: confronting arbitrary Higgs sectors with measurements at the Tevatron and the LHC. *Eur. Phys. J. C* **74**, 2711 (2014). <https://doi.org/10.1140/epjc/s10052-013-2711-4>. [arXiv:1305.1933](https://arxiv.org/abs/1305.1933)
78. P. Bechtle, S. Heinemeyer, O. Stål, T. Stefaniak, G. Weiglein, Probing the Standard Model with Higgs signal rates from the Tevatron, the LHC and a future ILC. *JHEP* **11**, 039 (2014). [https://doi.org/10.1007/JHEP11\(2014\)039](https://doi.org/10.1007/JHEP11(2014)039). [arXiv:1403.1582](https://arxiv.org/abs/1403.1582)
79. P. Bechtle, S. Heinemeyer, T. Klingl, T. Stefaniak, G. Weiglein, J. Wittbrodt, HiggsSignals-2: probing new physics with precision

- Higgs measurements in the LHC 13 TeV era. *Eur. Phys. J. C* **81**, 145 (2021). <https://doi.org/10.1140/epjc/s10052-021-08942-y>. [arXiv:2012.09197](https://arxiv.org/abs/2012.09197)
80. A. Djouadi, J. Kalinowski, M. Spira, HDECAY: a program for Higgs boson decays in the standard model and its supersymmetric extension. *Comput. Phys. Commun.* **108**, 56 (1998). [https://doi.org/10.1016/S0010-4655\(97\)00123-9](https://doi.org/10.1016/S0010-4655(97)00123-9). [arXiv:hep-ph/9704448](https://arxiv.org/abs/hep-ph/9704448)
81. HDECAY Collaboration, HDECAY: twenty₊₊ years after. *Comput. Phys. Commun.* **238**, 214 (2019). <https://doi.org/10.1016/j.cpc.2018.12.010>. [arXiv:1801.09506](https://arxiv.org/abs/1801.09506)
82. ATLAS Collaboration, Search for resonant and non-resonant Higgs boson pair production in the $b\bar{b}\tau^+\tau^-$ decay channel using 13 TeV pp collision data from the ATLAS detector. *JHEP* **07**, 040 (2023). [https://doi.org/10.1007/JHEP07\(2023\)040](https://doi.org/10.1007/JHEP07(2023)040). [arXiv:2209.10910](https://arxiv.org/abs/2209.10910)